# Ligand field spectroscopy of Cu(II) and Ag(II) complexes in the gas phase: theory and experiment

**Ljiljana Puškar,[a] Hazel Cox,*[a] Alan Goren,[b] Georgina D. C. Aitken[a] and Anthony J. Stace*[a]**

[a] *School of Chemistry, Physics and Environmental Science, University of Sussex, Falmer, Brighton, UK BN1 9QJ*

[b] *Department of Chemistry, Transylvania University, Lexington, Kentucky 40508, USA*

***Received 18th December 2002, Accepted 5th February 2003***
***First published as an Advance Article on the web 29th May 2003***

Ligand field spectra have been recorded in the gas phase for the two series of complexes containing either Cu(II) or Ag(II) in association with pyridine. Where comparisons are possible, the gas phase spectra match those recorded in the condensed phase; however, for Ag(II) systems the results differ in interpretation. The Ag(II) data are attributed to a ligand-to-metal charge transfer process, and the Cu(II) data (spectral region and extinction coefficient) match the characteristics of a d–d transition. A detailed theoretical analysis of two complexes, $[Cu(py)_4]^{2+}$ and $[Ag(py)_4]^{2+}$ provides evidence of a minimum energy, $D_{4h}$ structure and two less stable $D_{2h}$ and $D_{2d}$ structures within ~60 kJ mol$^{-1}$. From these structures it is possible to identify a range of optically and vibronically allowed transitions that could contribute to spectra observed in the gas phase. In the case of calculations on $[Ag(py)_4]^{2+}$ there is strong evidence of an electronic transition that would account for the observation of charge transfer in the experiments. Less detailed calculations on $[Cu(py)_6]^{2+}$ and $[Ag(py)_6]^{2+}$ show structural evidence of extensive Jahn–Teller distortion. Taken together with incremental binding energies calculated for complexes containing between two and six pyridine molecules, these results show that the level of theory adopted is capable of providing a semi-quantitative understanding of the experimental data.

## 1 Introduction

Ligand field spectroscopy is traditionally undertaken in the condensed phase, which means that the presence of a counter ion, and (quite often) a solvent, restricts the degree to which accurate correlations can be made between electron configuration, spectral transitions, and the structure of the chromophore.[1,2] For measurements performed in solution, inhomogeneous broadening coupled with low frequency vibrational modes leads to very broad spectral bands that can frequently embrace several electronic transitions, even to the point where spin–orbit splittings can not be resolved. This situation contrasts markedly with the significant advances that have been made in the spectroscopy of size-selected metal ion complexes in the gas phase.[3] However, these latter experiments have until recently been restricted to singly charged species, whereas many of the more important metal ion complexes in condensed phase chemistry and biochemistry are multiply charged.[1,2,4]

Since isolated multiply charged metal ions, for example $Cu^{2+}$, are unstable in the gas phase with respect to collision-induced charge transfer with almost all molecules, the preparation of stable transition metal complexes, for example $[Cu(H_2O)_n]^{2+}$, has presented a considerable technical challenge. To date, two complementary experimental techniques have emerged. Using electrospray, a number of groups have been successful in generating a range of doubly and triply charged complexes.[5–9] This approach appears to work particularly well for structural studies of biologically-related ligands;[7] however, Posey *et al.*[8] and Thompson *et al.*[9] have also demonstrated that the technique is capable of yielding information on the electronic spectroscopy of doubly charged complexes. We have recently developed an alternative to electrospray that relies on a pick-up process to generate neutral metal/ligand complexes, which are then ionised by high energy electron impact.[10–16] The resultant complexes do not undergo charge transfer because, at the time of formation, the multiply charged metal ions are encapsulated in a stabilising solvent environment. Thus far, the technique has been used to prepare transition metal complexes containing Cu(II),[10,13,14] Cr(II),[16] Mn(II),[15] Ag(II),[11,13] and Au(II),[12,13] and has the advantage of being able to accommodate a very diverse range of ligands.

One of the most significant goals in any series of experiments on gas phase transition metal complexes has to be that of studying their ligand field spectroscopy. Such studies would enable the development of a ligand field to be interrogated in the absence of any perturbations from either counter ions or solvents. In principle, it should be possible to achieve the level of spectroscopic detail currently realised for large molecules and small clusters using photofragmentation techniques in the gas phase, *i.e.* vibrational state resolution and the analysis of rotational band contours.[3]

However, apart from problems associated with the generation of stable complexes, spectroscopic measurements of ligand field transitions present additional experimental challenges in the form of very low extinction coefficients.[1] Despite these problems, new data are beginning to emerge,[8,9] and presented below are the results of measurements of ligand field transitions in Cu(II) and Ag(II) systems. Some of the complexes have been the subject of a study of charge transfer transitions at UV wavelengths,[17] and a preliminary report on d–d spectra recorded for $[M(py)_4]^{2+}$ complexes has also been presented.[18]

It is very unlikely that experiments of the type described here will achieve an accuracy whereby rotational energy contour analysis can yield a complete structure; at best it may be possible to distinguish square-planar from tetrahedral. Therefore, an important aspect to this study is the implementation of theoretical methods capable of calculating ground and excited state energy level differences, which together with knowledge of symmetry-allowed transitions can be used to reproduce (stick) spectra. At some future stage the calculation of oscillator strengths will be included to complete the picture.

For some examples, it has been possible to perform experiments on complexes, *e.g.* $[Cu(py)_4]^{2+}$ and $[Ag(py)_4]^{2+}$, at wavelengths that have been the subject of spectral measurements in the condensed phase.[19–25] In several instances, there is a close match between spectra from the two sources; however, in some cases the interpretation of results is quite different from that given previously.

## 2 Experimental section

A detailed description of the instrumentation used to generate and detect cationic metal complexes has been provided in previous publications.[11,14] Briefly, neutral metal/solvent clusters were ionised by 100 eV electrons within the ion source of a high resolution, double focusing mass spectrometer (VG ZAB-E), and were then accelerated by a potential of +5 kV. After passing through a field-free region, ions were selected according to their mass/charge ratio using a magnet. These ions then entered a long field-free region (~1.5 m) of the mass spectrometer where they were irradiated with the output of two separate laser systems. An OPO (optical parametric oscillator) laser (Spectra-Physics MOPO-710) pumped with an injection-seeded Nd:YAG laser (Spectra-Physics GCR-200) was used to cover the wavelength ranges 440–690 nm (signal) and 730–1200 nm (idler). Laser radiation with a tuning range of 220–310 nm was generated by frequency-doubling the output from a dye laser (SIRAH–PrecisionScan) pumped with a Nd:YAG laser (Surelite III) operating at 355 nm. Data points at a single wavelength represent an average of 3000–4000 laser shots, and many of the spectra shown took up to 24 h of continuous measurement to record.

## 3 Computational details

The calculations were performed using the Amsterdam density functional (ADF) package[26] in association with the numerical integration procedure of te Velde and Baerends.[27] A triple-ζ Slater-type-orbital (STO) basis set with a polarisation function (TZP) was used to describe the valence electrons of each atom: Cu (3s 3 p 3 d 4 s), Ag (4 s 4 p 4 d 5 s), C (2 s 2 p) and N(2 s 2 p), and electrons in lower shells were treated with the frozen core approximation. The energies of structures were calculated using the local density approximation (LDA) due to Vosko *et al.*[28] with the non-local exchange terms of Becke,[29] and with the non-local correlation correction of Perdew being applied to the calculated LDA densities.[30]

To estimate electronic transition energies, standard density functional techniques were used to explore the lowest lying energy states of each spatial irreducible representation of the system, since they represent 'ground state' in that particular symmetry.[31] This could be accomplished within ADF by simply assigning the appropriate number of electrons to each irreducible representation within a point group symmetry, then setting up the Kohn–Sham determinants, and computing the energy difference between the assigned state and the ground state configuration (this approach is frequently referred to as the ΔSCF method). The results of unrestricted calculations on these $d^9$ doublet systems were shown to be quantitatively similar to those obtained from less demanding restricted calculations. Thus, all excitations were performed using restricted calculations so that a pure spatial transition could be determined (as opposed to concerning ourselves with transition energies between appropriate spins, *i.e.*, $\beta \rightarrow \beta$). Recent calculations by Deeth[32] and Szilagyi *et al.*[33] suggest that DFT can overestimate the degree of covalency in Cu(II) complexes. As a result, the energies of d–d electronic transitions are predicted to be too high. We shall address this point later in the discussion.

Allowed electronic transitions were determined using group theoretical methods. In order to preserve the doublet spin state, it was assumed that all transitions would involve either a pairing of the single electron in the HOMO or a transition from the HOMO to an unoccupied orbital such as the LUMO. Both electric dipole allowed and vibronic transitions were considered, although it is acknowledged that the intensities of the latter are likely to be considerably weaker than the former.[1]

Spectral transition probabilities are determined by whether or not symmetry considerations require a matrix element to vanish. In general the intensity, $I$, of a transition from one state $\varphi_i$ to another $\varphi_j$ is given by an equation of the form:

$$I \propto [\int \varphi_i \mu \varphi_j \mathrm{d}\tau]^2$$

where $\mu$ is a transition moment operator, which in this case is the electric dipole operator. An electric dipole-allowed transition can acquire intensity from any of three directions $x$, $y$ or $z$, depending on the polarization of the light, and a transition will be allowed if the direct product of the representations of the two states concerned is or contains the irreducible representation to which $x$, $y$ or $z$, respectively, belongs. The laser radiation used in these experiments is polarized, and although the cations being excited are randomly orientated in space, it is possible to observe the consequences of changing the plane of polarization on photofragmentation patterns.[34] However, signal intensities were not high enough to perform that type of experiment on the metal cations.

Interest in these particular experiments is primarily associated with the possibility of observing d–d transitions, which are formally forbidden in molecules with inversion symmetry. Since all d-orbitals are symmetric to inversion, a *gerade–gerade* transition will always be forbidden because the dipole moment operator is anti-symmetric, therefore a direct product with two *gerade* states will never produce a totally symmetric state. However, with the inclusion of vibronic coupling between vibrational and electronic wave functions, the states of the $d^n$ configuration no longer retain their *gerade* character, and transitions become "allowed". Following from group theory, an integral will be non-zero if there is a normal mode of vibration with a first excited state belonging to one of the representations spanned by $\varphi_i \mu \varphi_j$. As an example, in $D_{4h}$, a $B_{1g} \leftarrow B_{2u}$ transition is dipole allowed (as $B_{1g} \otimes B_{2u} = A_{2u}$) but $B_{1g} \leftarrow A_{1g}$ is not. However, if $A_{1g} \otimes B_{2u}$ is a member of the normal modes of $D_{4h}$ then $A_{1g}$ can borrow intensity from $B_{2u}$ to make the transition to $B_{1g}$. In fact,

$A_{1g} \otimes B_{1g} = B_{1g}$ and $B_{1g}$ is a normal mode of a $D_{4h}$ $ML_4$ molecule and so $B_{1g} \leftarrow A_{1g}$ will be vibronically allowed. In the results section allowed transitions have been divided into two groups: those that are optically allowed and those that are allowed through vibronic coupling.

## 4 Experimental results

### 4.1 Visible spectra for $[Cu(py)_n]^{2+}$ and substituted pyridines

In the condensed phase, König and Schläfer[20,21] have recorded reflectance spectra for $[CuX_2(py)_2]$, (X = Cl,Br) complexes in the 240–1000 nm region. Each spectrum comprises of three distinct bands: at long wavelengths there is a maximum at ~700 nm which is assigned to a d–d transition. A pyridine centred $\pi \rightarrow \pi^*$ transition is thought to be responsible for absorption seen at short wavelengths (~260 nm), and an intense band lying between 300 and 400 nm is assigned as a metal-to ligand (electron) charge transfer (MLCT) transition from a d orbital on $Cu^{2+}$ to an empty $\pi^*$ orbital of pyridine. The positions of both the d–d and pyridine-centred $\pi \rightarrow \pi^*$ transitions were found to be independent of X (X = Cl,Br).

The photoexcitation of mass selected $[Cu(py)_n]^{2+}$ complexes ($n$ = 2–7) at wavelengths between 450 and 1100 nm lead to the following fragmentation pathways:

$$[Cu(py)_2]^{2+} \rightarrow \text{no observed fragmentation} \quad (1)$$

$$[Cu(\ py)_3]^{2+} \rightarrow Cu^+(py)_2 + py^+ \quad (2)$$

$$[Cu(py)_n]^{2+} \rightarrow [Cu(py)_{n-1}]^{2+} + py \ \{\text{for } n = 4\text{–}6\} \quad (3)$$

$$[Cu(py)_7]^{2+} \rightarrow [Cu(py)_5]^{2+} + 2(py) \quad (4)$$

Within the given wavelength range no photofragments were detected from the $[Cu(py)_2]^{2+}$ complex, even though the ion had an intensity comparable to those recorded for $n = 6$ and $n = 7$. Similarly for $n = 3$, data had to be accumulated for over 10,000 laser shots to distinguish between the weak laser-induced signal and complementary fragmentation induced through metastable decay. The only photofragmentation channel detected was the loss of one charged pyridine ($py^+$) to leave a stable $Cu^+(py)_2$ unit[2] which is consistent with the results of collisional activation experiments.[14]

Photodissociation of $[Cu(py)_n]^{2+}$ cluster ions, in the range $n$ = 4–6, was observed with the loss of one pyridine molecule as the only fragmentation route. For complexes with $n = 7$ the photon energy was sufficient to break two pyridine bonds and $[Cu(py)_5]^{2+}$ was the only ionic photofragment observed. Photofragment yields for $n$ = 4–6 were sufficiently high as to enable spectra to be recorded as a function of laser wavelength. Fig. 1 shows examples of spectra recorded over the 10,000–20,000 $cm^{-1}$ energy range. Each data point is the average of ~4,000 laser shots, and the spectra have been normalised with respect to both laser power and fluctuations in the parent ion intensities. The energy gap of 794 $cm^{-1}$ represents a region where laser output switches between the signal and the idler output and no radiation is available over this range.

If it is assumed that the absorption of a single photon by each complex always leads to photodissociation, then a photofragment spectrum should reflect an absorption spectrum. The only circumstance under which that assumption may breakdown is when the binding energy of a ligand becomes larger than the energy of a photon. However, internal excitation as a result of the method used to generate the ions, may blur that boundary. Although an accurate measurement of absorption cross sections was not possible, primarily due to the uncertainty of the length of the overlap between the laser and the cluster beam in the second field free region (2nd ffr) of the mass spectrometer, an estimate of the extinction coefficient for $[Cu(py)_4]^{2+}$ was obtained. The photo-induced depletion of the $[Cu(py)_4]^{2+}$ ion signal was compared to that for $Ar_3^+$ under precisely the same experimental conditions. Both experimental and theoretical values of the $Ar_3^+$ photo-absorption cross section are well-documented,[35–37] and argon clusters are always present in the ion beam as part of the technique for producing metal complexes. It was, therefore, possible to switch from the $[Cu(py)_4]^{2+}$ signal to that of $Ar_3^+$ without changing the overlap between the laser and the

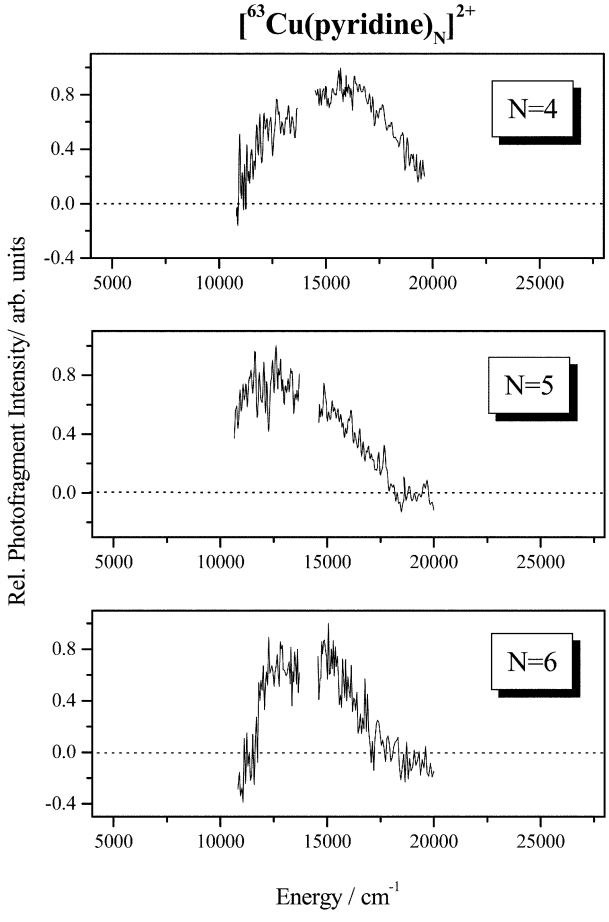


**Fig. 1** Absorption spectra recorded by monitoring the photofragmentation yields of size-selected $[Cu(py)_n]^{2+}$ complexes as a function of laser wavelength. Data are presented for $n$ in the range 4–6.

cluster ion beam. An extinction coefficient of $\varepsilon \sim 100$ L mol$^{-1}$ cm$^{-1}$ was determined for $[Cu(py)_4]^{2+}$ at 600 nm with an uncertainty of *ca.* 50%.

The photofragment spectrum recorded for $[Cu(py)_4]^{2+}$ (top panel, Fig. 1) closely resembles the long-wavelength absorption band recorded by König and Schläfer.[20,21] Overall, the data given in Fig. 1, suggest the presence of a small spectral shift to lower energies as the number of pyridine molecules is increased from $n = 4$ to $n = 6$, and the shift is most pronounced with the addition of a fifth pyridine molecule. By varying solvent conditions in order to enhance the equilibrium concentrations of specific cations, two groups have succeeded in recording absorption spectra for different-sized $[Cu(py)_n]^{2+}$ complexes. Leussing and Hansen[19] recorded spectra for $n \leq 5$ covering the wavelength range 600–850 nm. The characteristic profile of their absorption feature for $n = 4$ is similar to that given in Fig. 1 for $[Cu(py)_4]^{2+}$. Measurements by Ozutsumi and Kawashima[24,25] for $n \leq 4$ show a similar pattern of behaviour over the wavelength range 300–900 nm. However, both studies noted that the uptake of successive pyridine molecules was accompanied by a progressive shift of the absorption maximum towards the blue;[21–23] a trend which contrasts with the results shown in Fig. 1. In related work on Cu(II)/ammonia complexes, Bjerrum *et al.*[38] observed a gradual shift towards the blue with the uptake of successive ammonia molecules until $n = 4$, after which a fifth ammonia reversed the trend and shifted the absorption maximum towards the red. Similar behaviour has been seen with ethylenediamine as a ligand.[39] Leussing and Hansen[19] rationalised their conflicting data by suggesting that, of the three ligands, pyridine is more strongly

bound to Cu(II), and that this leads to a greater splitting of the 3d orbitals as a consequence of a larger ligand field interaction.

Ozutsumi and co-workers[24] also studied the structures of Cu(II)/pyridine complexes in aqueous solution using the extended X-ray absorption fine structure (EXAFS) technique. Comparing $[Cu(H_2O)_6]^{2+}$ and $[Cu(py)_n(H_2O)_{6-n}]^{2+}$, they found the axial Cu–O bond to increase in length as the value of $n$ increased up to four. The proposed explanation was based on steric repulsion from the pyridine molecules and that at $n = 4$, the molecular plane of the pyridine was not parallel to the equatorial plane of the complex. Analogous interaction in, for example, $[Cu(py)_{5,6}]^{2+}$ would presumably destabilise the axial pyridine molecules (see below).

The extinction coefficient measured for $[Cu(py)_4]^{2+}$ in the gas phase compares favourably with values recorded for spin allowed d–d transitions in Cu(II) complexes in aqueous solution.[1,19,24] This together with a marked similarity between the various absorption profiles as a function of wavelength, suggests that a ligand field d–d transition into the antibonding $d_{x^2-y^2}$ orbital is responsible for the observed absorption spectra for $[Cu(py)_n]^{2+}$ complexes in the gas phase.

The influence of pyridine substitution on the photofragmentation spectra of Cu(II) complexes was investigated over the same wavelength region using 4-methyl-pyridine (4-picoline). The presence of an electron donating methyl group group at the *para* position to the nitrogen atom makes 4-picoline a stronger base ($pK_a = 6.08$) than unsubstituted pyridine ($pK_a = 5.18$). Therefore, the greater availability of σ electron density on the nitrogen atom may influence bonding to the metal cation. Likewise, changes in π electron density could have an effect on the degree of back-bonding between the metal and the pyridine ring. The marked change in basicity implies that a difference in σ electron density might be the dominant effect when comparing pyridine with 4-picoline.

The parent ion intensity distribution of $[Cu(4\text{-pic})_n]^{2+}$ complexes was consistent with that recorded previously for pyridine, with $n = 4$ being the most intense ion. Photofragment dissociation channels were investigated for $[Cu(4\text{-pic})_n]^{2+}$ complexes in the range $n = 3$–6, and were found to be very similar to those recorded for $[Cu(py)_n]^{2+}$. The photodissociation of $[Cu(4\text{-pic})_3]^{2+}$ proceeded *via* the loss of one $(4\text{-picoline})^+$ ion, but was too low in intensity to permit a photofragmentation spectrum to be recorded. The positions of the absorption bands measured for $[Cu(4\text{-picoline})_n]^{2+}$ complexes appear slightly blue shifted with respect to those recorded for pyridine over the same size range. In a related study of $Ni(X\text{-py})_4(ClO_4)_2$ complexes and with a range of substituent X on pyridine, Bull and Moore concluded that the effects of substitution at the 3- and 4-positions were too small to influence the magnitude of the ligand field splitting constant, $\Delta$.[41] As for $[Cu(py)_n]^{2+}$ complexes, the addition of a fifth and sixth molecule to $[Cu(4\text{-picoline})_4]^{2+}$ shifts the absorption band to lower energies; however, the observed red shift for $[Cu(4\text{-picoline})_5]^{2+}$ is less pronounced (~1,400 $cm^{-1}$) than for $[Cu(py)_5]^{2+}$ (~2,500 $cm^{-1}$).

### 4.2 Visible spectra for $[Ag(py)_n]^{2+}$ and substituted pyridines

Although Ag(II) complexes are frequently unstable in solution, they can often be stabilised with nitrogen-containing heterocyclic organic ligands such as pyridine and pyridine derivatives.[22,42,43] These complexes frequently exhibit four coordination and examples, such as $[Ag(py)_4]S_2O_8$, are reported to be square planar.[22,42] On moving from the first to the second row of the d-block, the valence shell 4d orbitals become more spatially extended and the degree of overlap between these orbitals on the metal and those on the ligands orbitals is frequently assumed to increase (see below). This behaviour is thought to be responsible for shifting ligand field transition energies to shorter wavelengths in $4d^n$ metal cations when compared with $3d^n$ cations. In the condensed phase, $\lambda_{max}$ is ~470 nm for $[Ag(py)_4]S_2O_8$,[22] which is to be compared with ~600 nm for a typical Cu(II)/pyridine complex.[1]

For the clusters in the range of $n = 2$–7, photofragmentation patterns were investigated over the wavelength range 450–1100 nm. At all values of $n$ except 2, absorption was observed at wavelengths between 450 and 650 nm, which resulted in the following photofragmentation channels:

$$[Ag(py)_3]^{2+} \rightarrow Ag(py)^+ + py^+ + py \quad (5)$$

$$[Ag(py)_4]^{2+} \rightarrow Ag(py)_2{}^+ + py^+ + py \quad (6)$$

$$[Ag(py)_5]^{2+} \rightarrow [Ag(py)_4]^{2+} + py \quad (7)$$

$$[Ag(py)_6]^{2+} \rightarrow [Ag(py)_4]^{2+} + 2\ py \quad (8)$$

There are marked differences between these fragmentation channels and those recorded for $[Cu(py)_n]^{2+}$ complexes, which for the most part, proceeded *via* the loss of one *neutral* pyridine molecule in the size range of $n = 4$–6. In particular, the observation of two charged fragments $py^+$ and $[Ag(py)_2]^+$ from the $[Ag(py)_4]^{2+}$ complex would suggest that photon absorption is accompanied by electron transfer; the implication being that at visible wavelengths, $[Ag(py)_4]^{2+}$ undergoes ligand-to-metal charge (electron) transfer (LMCT). In their analysis of $[Ag(py)_4S_2O_8]$ spectra, Banerjee and Basu discussed the possibility of a charge transfer contribution at short wavelengths (~450 nm).[22]

Unlike the photofragmentation patterns seen for $[Cu(py)_6]^{2+}$, the complex $[Ag(py)_6]^{2+}$, responds to excitation by losing two pyridine molecules, to leave a stable $[Ag(py)_4]^{2+}$ unit. The photon energy is therefore sufficient to break two metal – ligand bonds in $[Ag(py)_6]^{2+}$, rather than one as seen for the corresponding Cu(II) complex. Such behaviour could be as a consequence of the greater degree of Jahn–Teller distortion associated with Ag(II) $d^9$ complexes, with the two axial ligands being displaced significantly further than the four equatorial ligands from the ion core (see below). In a theoretical study of hexahydrated first and second row transition metal ions, Åkesson *et al.*[44] reported both the $Cu^{2+}$ and $Ag^{2+}$ hydrates to be Jahn–Teller distorted structures with tetragonal elongation. Calculated silver–oxygen distances, at both axial ($R_{ax} = 2.48$ Å) and equatorial ($R_{eq} = 2.22$ Å) positions were found to be longer than the corresponding Cu–O distances ($R_{ax} = 2.24$ Å; $R_{eq} = 2.06$ Å).[11] With reference to results given below, it should be noted that Åkesson *et al.*[44] also reported a total binding energy for Ag(II) hydrate as 1155 kJ $mol^{-1}$, which is to be compared with 1344 kJ $mol^{-1}$ for the correspond Cu(II) complex. These calculated data follow the same trend as the single-ion hydration enthalpies.[45]

Fig. 2 shows photofragmentation spectra recorded for $[Ag(py)_n]^{2+}$ ($n = 4$–6). The spectrum for $[Ag(py)_4]^{2+}$ compares favourable with those recorded previously in the condensed phase for $[Ag(py)_4]S_2O_8$. Likewise, the shift in $\lambda_{max}$ relative to $[Cu(py)_4]^{2+}$ is also comparable to that seen in the analogous condensed phase complexes.[22,42] The spectra recorded for $[Ag(4\text{-pic})_5]^{2+}$ and $[Ag(py)_{5,6}]^{2+}$ are nearly identical with absorption maxima at ~21,000 $cm^{-1}$. A somewhat larger blue shift could possibly be ascribed to $[Ag(4\text{-pic})_4]^{2+}$ as the spectrum appears to peak at higher energies than are available in these experiments. Wasson[42] examined the influence of 3- and 4-picoline substitution on tetra-coordinated Ag(II) complexes by comparing their visible absorption spectra with that of the square planar tetrapyridine silver(II) persulfate, $Ag(py)_4S_2O_8$.[42] The picoline complexes exhibited a small blue shift in the order: $Ag(py)_4S_2O_8$($\lambda_{max} = 400$ nm), $Ag(3\text{-pic})_4S_2O_8$ ($\lambda_{max} = 380$ nm) and $Ag(4\text{-pic})_4S_2O_8$ ($\lambda_{max} = 370$ nm). The shift was found to follow the order of the basicity of the ligands (4-pic > 3-pic > py), rather than that of any π-donor contribution from the substituent, which would be in the order 3-pic > 4-pic > py.[46] However, it was similarly concluded that substitution at 3- and 4- position on the pyridine ring has very little, if any effect on the energy of any ligand field transitions. Consistent with the observations of Wasson,[42] 4-methyl substitution appears to have negligible influence on the visible spectra presented here for Ag(II)/pyridine complexes.

In an early study by Banerjee and Basu[22] of the spectrum of $[Ag(py)_4]S_2O_8$ in the condensed phase the absorption profile was resolved into three Gaussian components each of which was assigned to d–d transitions appropriate for a $d^9$ square planar configuration. However, the results shown here covering the same wavelength range provide strong evidence of a charge transfer transition in Ag(II) pyridine/4-picoline complexes. The formation of charged fragments upon irradiation of the $n = 4$ complex could be as a consequence of direct promotion of an electron from Ag–N ligand bond to the half-empty $d_{x^2-y^2}$ orbital of a square planar complex. Since the transition is into an antibonding orbital it would favour immediate dissociation to produce $py^+$ and $[Ag(py)_3]^+$. Some fraction of the resultant repulsive Coulomb energy could subsequently promote the loss of neutral pyridine to form the more stable $[Ag(py)_2]^+$ ion.[2] Additional support for this route comes from the estimated value for the extinction coefficient. For ligand field transitions in square planar and octahedral complexes, molar extinction coefficients are usually $< 100$ L $mol^{-1}$ $cm^{-1}$[11,20,47] (see for example the value quoted above for $[Cu(py)_4]^{2+}$). In contrast, charge transfer

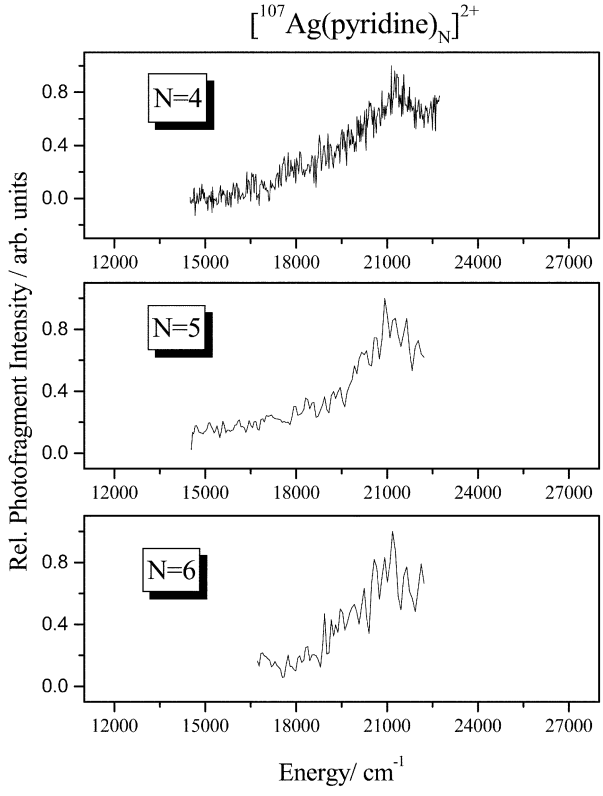


**Fig. 2** Absorption spectra recorded by monitoring the photofragmentation yields of size-selected $[Ag(py)_n]^{2+}$ complexes as a function laser wavelength. Data are presented for $n$ in the range 4–6.

transitions are usually optically allowed and, as such, have extinction coefficients that are typically $\geq$1000 L mol$^{-1}$ cm$^{-1}$.[1] Using the same method described earlier for Cu(II) complexes, an extinction coefficient of ~500 L mol$^{-1}$ cm$^{-1}$ has been estimated for $[Ag(4\text{-picoline})_4]^{2+}$.

An alternative route to photodissociation would be for photoexcitation to promote a d–d transition, which would lead to the loss of neutral pyridine and leaving an unstable doubly charged $[Ag(py)_3]^{2+}$ ion.[11] This ion would then undergo immediate electron transfer to give $[Ag(py)_2]^{+}$ and $py^{+}$. Since these two events are likely to be coupled, the mixing of excited states should introduce a charge transfer component into the initial excitation process.

## 5 Calculated results and discussion

### 5.1 Structures and binding energies

Calculations have been performed on all $[M(py)_n]^{2+}$ complexes, where M is either Cu or Ag and $n$ lies in the range 1–6. Since the main interest in this paper is to interpret electronic spectra recorded for $[M(py)_{4,5,6}]^{2+}$ complexes, most attention will be paid to presenting the results of calculations on these structures. However, to place that data in context, selected results will also be presented for the complete range of different-sized complexes. Relative energies for each of three (obvious) trial geometries for $[M(py)_4]^{2+}$ and $[M(py)_6]^{2+}$ configurations are given in Table 1. As can be seen, the $[M(py)_4]^{2+}$ complexes have $D_{4h}$ ground state structures and that there are two other geometries, $D_{2h}$ and $D_{2d}$, lying within 60 kJ mol$^{-1}$. For $[M(py)_6]^{2+}$ complexes, there are again three possible geometries, all with an overall symmetry of $D_{2h}$, but having different ligand orientations depending on how they are constructed from the underlying $[M(py)_4]^{2+}$ unit. For $[Cu(py)_6]^{2+}$ the ground state

**Table 1** Total binding energy of structures calculated for $[M(pyridine)_4]^{2+}$ and $[M(pyridine)_6]^{2+}$ complexes. The energy of each configuration is relative to the most stable isomer and the units are kJ $mol^{-1}$

| | $[Cu(pyridine)_4]^{2+}$ | | $[Ag(pyridine)_4]^{2+}$ | |
|---|---|---|---|---|
| Symmetry | Restricted | Unrestricted | Restricted | Unrestricted |
| $D_{4h}$ | 0.0 | 0.0 | 0.0 | 0.0 |
| $D_{2h}$ | 33.9 | 36.0 | 16.4 | 18.7 |
| $D_{2d}$ | 34.0 | 38.3 | 57.1 | 59.5 |
| Symmetry | $[Cu(pyridine)_6]^{2+}$ | $[Ag(pyridine)_6]^{2+}$ | | |
| **6A**: $D_{2h}$ ($ML_4$ $D_{4h}$) | 0.0 | 13.8 | | |
| **6B**: $D_{2h}$ $\parallel$ ($ML_4$ $D_{2h}$)[a] | 57.4 | 47.7 | | |
| **6C**: $D_{2h}$ $\perp$ ($ML_4$ $D_{2h}$)[b] | 16.8 | 0.0 | | |

[a] Parallel to the plane formed by the $ML_4$ structure. [b] Perpendicular to the plane formed by the $ML_4$ structure.

structure is derived from the $D_{4h}$ stable unit; but for $[Ag(py)_6]^{2+}$ there is a switch in geometry, and a structure derived from an underlying $D_{2h}$ configuration becomes the most stable geometry. Examples of the various geometries are shown in Fig. 3.

Table 2 gives M–N bond lengths derived from the calculations, and there are two significant observations to be made from these data. First, the M–N distances are longer for Ag(II)-containing structures than for those based on Cu(II); this result reflecting the larger ionic radius of the $Ag^{2+}$ ion. Secondly, the M–N bonds in $[M(py)_6]^{2+}$ complexes for both metal cations experience considerable Jahn–Teller distortion. In at least two of the geometries, the distorted M–N bonds are comparable in length to molecular distances more typically associated with van der Waals complexes rather than ionic solids. This latter observation is underpinned by the relative binding

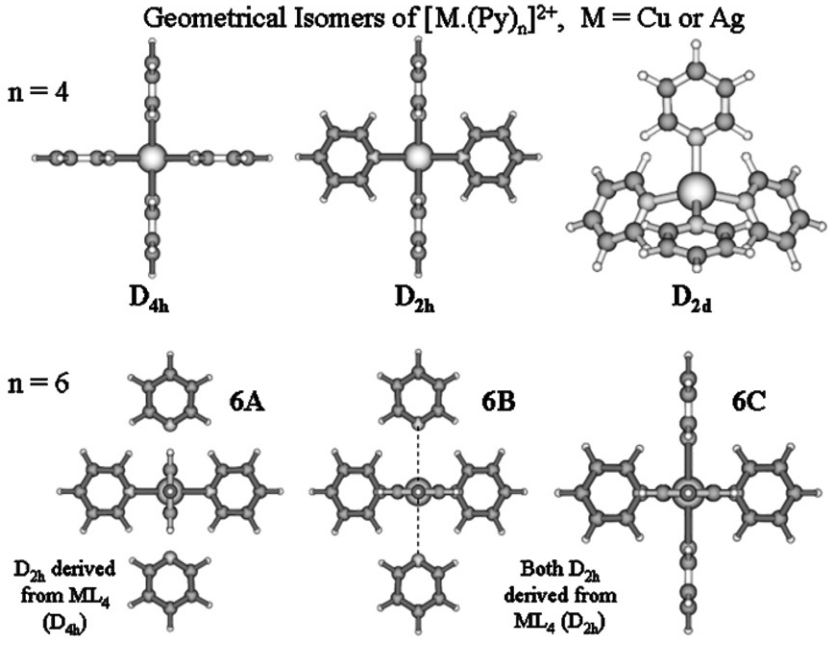


**Fig. 3** Stable structures calculated for $[M(py)_4]^{2+}$ and $[M(py)_6]^{2+}$ complexes, where M is either Cu or Ag. The relative energy differences are given in Table 1 and the M–N bond distances are given in Table 2.

**Table 2** Metal–nitrogen bond lengths in $[M(pyridine)_4]^{2+}$ and $[M(pyridine)_6]^{2+}$ complexes

| Complex | Symmetry | Cu–N/Å | Ag–N/Å |
|---|---|---|---|
| $[M(py)_4]^{2+}$ | $D_{4h}$ | 1.97 | 2.19 |
| | $D_{2h}$ | 1.95 ⊥, 2.08 \|\| | 2.16 ⊥, 2.26 \|\| |
| | $D_{2d}$ | 1.99 | 2.20 |
| $[M(py)_6]^{2+}$ | **6A**: $D_{2h}$ ($D_{4h}$) | 1.95, 1.97, 3.72 J–T[a] | 2.16, 2.22, 3.69 J–T |
| | **6B**: $D_{2h}$ \|\| | 1.91 ⊥, 2.09 \|\|, 3.73 J–T | 2.19 ⊥, 2.24 \|\|, 3.72 J–T |
| | **6C**: $D_{2h}$ ⊥ | 2.05 ⊥, 2.08 \|\|, 2.42 J–T | 2.23 ⊥, 2.26 \|\|, 2.57 J–T |

[a] Bond distance associated with Jahn–Teller distortion.

energies discussed below. For the $[Cu(py)_4]^{2+}$ $D_{4h}$ structure the calculated M–N bond length is to be compared with the result from EXAFS experiments by Ozutsumi and Kawashima who quote a value of 2.03 Å with a standard deviation of 0.06 Å.[24]

Fig. 4 gives a plot of the average binding energy as defined by: $[M(py)_n]^{2+} \rightarrow M^{2+} + n\,py$, and derived from the relative energies of each of the most stable structures in the series $[M(py)_n]^{2+}$ for $n = 1$–6. As can be seen, the calculations suggest that, of the two cations, $Ag^{2+}$ is more strongly solvated by pyridine. This result contrasts with both the observations of Åkesson *et al.*[44] on the hydrates of $Cu^{2+}$ and $Ag^{2+}$, and with values for the single-ion hydration enthalpies.[45] Data comparing $Cu^{2+}$ and $Ag^{2+}$ in solvents other than water does not appear to be available. Fig. 5 presents a plot of the incremental binding energies as defined by the difference: $[M(py)_n]^{2+} \rightarrow [M(py)_{n-1}]^{2+} + py$. Note the very low values for $n = 5$ and 6, which are as a consequence of the high degree of Jahn–Teller distortion in the parent complexes. A further point of interest is the unexpectedly large binding energy calculated for $[Cu(py)_4]^{2+}$ with respect to the loss of a single molecule. This energy is equivalent to a photon wavelength of ~450 nm (~20,000 $cm^{-1}$); in contrast, the binding energies of $n = 5$ and 6 translate as ~4000 $cm^{-1}$. Thus, the $n = 4$ complex needs to have an appreciable degree of internal excitation to photodissociate at $< 15{,}000$ $cm^{-1}$. In contrast, the red shift seen in Fig. 1 could be due to the ease with which $n = 5$ and 6 photodissociate at lower photon energies. However, in all circumstances, the ions are still required to have electronic transitions that are capable of excitation at the wavelengths used; what changes with residual internal energy is how effective the photon is at promoting dissociation. The data shown in Fig. 5 also provides an explanation for the difference in fragmentation pattern between $[Cu(py)_6]^{2+}$ (loss of one molecule) and $[Ag(py)_6]^{2+}$ (loss of two molecules). At ~12,500 $cm^{-1}$, the energy of a photon exciting $[Cu(py)_6]^{2+}$ is probably not sufficient to promote the loss of two molecules on the time scale of the experiment ($\sim 10^{-5}$ s). In contrast, photons being absorbed by $[Ag(py)_6]^{2+}$ at $\lambda_{max}$ have an energy of ~22,000 $cm^{-1}$, which is almost three times the calculated binding energy for two molecules.

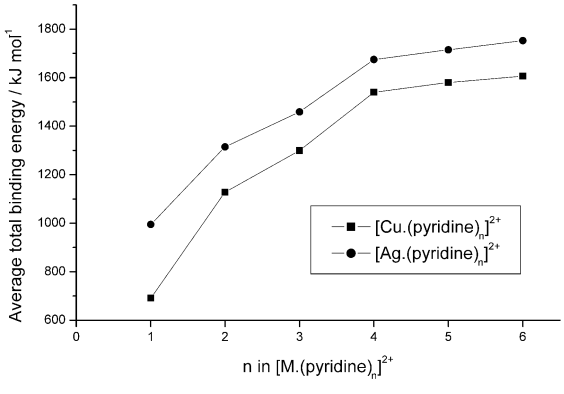


**Fig. 4** Average total binding energy calculated for $[M(py)_n]^{2+}$ complexes, where $n \leq 6$.

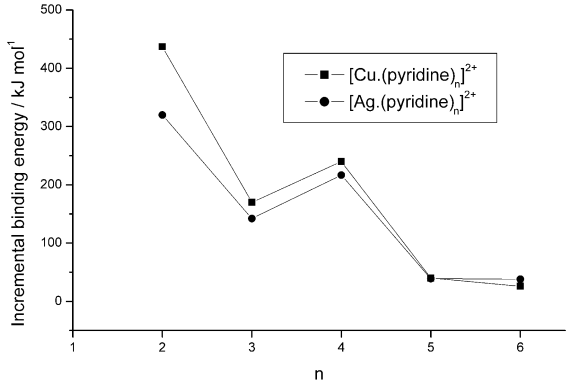


**Fig. 5** Incremental binding energy calculated from the energy difference $[M(py)_n]^{2+} \rightarrow [M(py)_{n-1}]^{2+} + py$.

Finally, Fig. 5 shows an unexpected fluctuation in the binding energies, in that the calculations predict that, for both metal cations, a molecule in a $[M(py)_4]^{2+}$ complex is more strongly bound than in a $[M(py)_3]^{2+}$ complex. The consequences of this result in an experiment involving the measurement of ion intensities in a mass spectrometer, would be for the $[M(py)_4]^{2+}$ ions to appear

**Table 3** List of the dipole-allowed electronic transitions calculated for $[Cu(pyridine)_4]^{2+}$ and $[Ag(pyridine)_4]^{2+}$ complexes for each of the three geometries shown in Fig. 3

| Metal | Point group | Dipole-allowed transition | Metal (%) | Ligand (%) | Transition energy/cm$^{-1}$ |
|---|---|---|---|---|---|
| Cu | $D_{4h}$ | HOMO $B_{1g}$ | 43 | 57 | 0 |
| | | $E_u \leftarrow B_{1g}$ | | 100 | 24 322 |
| | | $B_{1g} \leftarrow B_{2u}$ | | | 44 193 |
| | | $B_{1g} \leftarrow E_u$ | | 100 | 29291 |
| Ag | | Homo $B_{1g}$ | 32 | 68 | 0 |
| | | $E_u \leftarrow B_{1g}$ | | 100 | 22 100 |
| | | $B_{1g} \leftarrow B_{2u}$ | | 100 | 43 527 |
| | | $B_{1g} \leftarrow E_u$ | | 100 | 23 309 |
| Cu | $D_{2h}$ | HOMO $A_g$ | 43 | 57 | 0 |
| | | $B_{3u} \leftarrow A_g$ | | 100 | 26 300 |
| | | $A_g \leftarrow B_{1u}$ | | 100 | 31 624 |
| | | $A_g \leftarrow B_{2u}$ | | 100 | 33 303 |
| | | $A_g \leftarrow B_{3u}$ | | 100 | 29 233 |
| Ag | | HOMO $A_g$ | 33 | 67 | 0 |
| | | $B_{3u} \leftarrow A_g$ | | 100 | 27 705 |
| | | $A_g \leftarrow B_{1u}$ | | 100 | 26 910 |
| | | $A_g \leftarrow B_{2u}$ | | 100 | 27 057 |
| | | $A_g \leftarrow B_{3u}$ | | 100 | 23 320 |
| Cu | $D_{2d}$ | HOMO $B_2$ | 46 | 54 | 0 |
| | | $A_1 \leftarrow B_2$ | | 100 | 32 167 |
| | | $B_2 \leftarrow A_1$ | 49 | 51 | 12 003 |
| | | $B_2 \leftarrow A_1$ | 41 | 59 | 21 774 |
| | | $B_2 \leftarrow E$ | 48 | 52 | 6237 |
| | | $B_2 \leftarrow E$ | 7 | 93 | 15 830 |
| | | $B_2 \leftarrow E$ | 2 | 98 | 20 778 |
| | | $B_2 \leftarrow E$ | 31 | 69 | 24 162 |
| Ag | | HOMO $B_2$ | 31 | 69 | 0 |
| | | $A_1 \leftarrow B_2$ | | 100 | 14 331 |
| | | $B_2 \leftarrow A_1$ | 11 | 89 | 32 146 |
| | | $B_2 \leftarrow A_1$ | | | |
| | | $B_2 \leftarrow E$ | 15 | 85 | 8389 |
| | | $B_2 \leftarrow E$ | 12 | 88 | |

with intensities higher than their immediate neighbours. Similarly, the very low binding energies calculated for $n = 5$ and 6 would lead to these ions readily fragmenting, which would diminish their intensity and further enhance that of smaller ions, *i.e.* $[M(py)_4]^{2+}$. This pattern of behaviour is exactly what is observed in experiments on both $[Cu(py)_n]^{2+}$ and $[Ag(py)_n]^{2+}$ complexes.[11,14] Taken altogether this series of observations would suggest that the calculated binding energies have the correct magnitude and trend, and that Jahn–Teller distortion is having an influence on the outcome of photoexcitation.

As can be seen in Table 1, one of the structures, $D_{2d}$, calculated for $[Ag(py)_n]^{2+}$ lies significantly higher in energy than that of others containing either metal cation. Although significant internal excitation can result from the technique used to generate metal ion complexes, a geometry lying 60 kJ mol$^{-1}$ above the ground state is probably not going to be accessed as frequently as those at lower energies. Since the route to observing $[M(py)_4]^{2+}$ probably involves molecular evaporation from larger complexes, these process will lead to some cooling of the ions.

Tables 3 and 4 present a summary of electronic transition energies calculated for each of the three geometries identified for $[M(py)_4]^{2+}$ complexes. The transitions have been separated into two groups: dipole-allowed (Table 3) and those that are formally forbidden, but become parity allowed through vibronic coupling (Table 4). Although oscillator strengths have not been calculated, we have concentrated our analysis on the dipole-allowed transitions on the grounds that they should have greater intensity than those that require vibronic coupling to be observed. The dipole-allowed transitions have been summarised in Fig. 6 in terms of the relative energies of the orbitals concerned, where the transitions shown are restricted to those that may be accessible at visible wavelengths.

For copper(II) all geometries should be accessible during the course of an experiment; however, as can be seen from Table 3, many of the calculated transitions lie outside the range of our survey at visible wavelengths (10,000–23,000 cm$^{-1}$). If we are assuming that geometries ~30 kJ mol$^{-1}$

**Table 4** List of the vibronically-allowed electronic transitions calculated for $[Cu(pyridine)_4]^{2+}$ and $[Ag(pyridine)_4]^{2+}$ complexes for each of the three geometries shown in Fig. 3

| Metal | Point group | Vibronic transition | Metal (%) | Ligand (%) | Transition energy/cm$^{-1}$ |
|---|---|---|---|---|---|
| Cu | $D_{4h}$ | HOMO $B_{1g}$ | 43 | 57 | 0 |
| | | $B_{1g} \leftarrow A_{1g}$ | 76 | 24 | 27 044 |
| | | $B_{1g} \leftarrow A_{2g}$ | | 100 | 30 189 |
| | | $B_{1g} \leftarrow B_{1g}$ | | | 37 170 |
| Ag | | HOMO $B_{1g}$ | 32 | 68 | 0 |
| | | $A_{2g} \leftarrow B_{1g}$ | | 100 | 22 100 |
| | | $B_{1g} \leftarrow A_{1g}$ | 31 | 69 | 28 811 |
| | | $B_{1g} \leftarrow A_{2g}$ | | 100 | 30 161 |
| | | $B_{1g} \leftarrow A_{2u}$ | | 100 | 44 159 |
| | | $B_{1g} \leftarrow B_{1g}$ | 15 | 85 | 41 810 |
| Cu | $D_{2h}$ | HOMO $A_g$ | 43 | 57 | 0 |
| | | $A_g \leftarrow A_g$ | 80 | 20 | 24 241 |
| | | $A_g \leftarrow A_u$ | | 100 | 23 560 |
| | | $A_g \leftarrow B_{1g}$ | 39 | 61 | 20 724 |
| | | $A_g \leftarrow B_{2g}$ | 27 | 73 | 21 273 |
| | | $A_g \leftarrow B_{3g}$ | | 100 | 21 688 |
| Ag | | HOMO $A_g$ | 33 | 67 | 0 |
| | | $A_g \leftarrow A_g$ | 32 | 68 | 22 059 |
| | | $A_g \leftarrow A_u$ | | 100 | 19 315 |
| | | $A_g \leftarrow B_{1g}$ | 8 | 92 | 23 369 |
| | | $A_g \leftarrow B_{2g}$ | 0 | 100 | 21 074 |
| | | $A_g \leftarrow B_{3g}$ | | 100 | 21 067 |
| Cu | $D_{2d}$ | HOMO $B_2$ | 46 | 54 | 0 |
| | | $B_2 \leftarrow A_2$ | | 100 | 15 042 |
| | | $B_2 \leftarrow B_2$ | 2 | 98 | 21 741 |
| Ag | | HOMO $B_2$ | 31 | 69 | 0 |
| | | $B_2 \leftarrow A_2$ | | 100 | |
| | | $B_2 \leftarrow B_2$ | | 100 | |

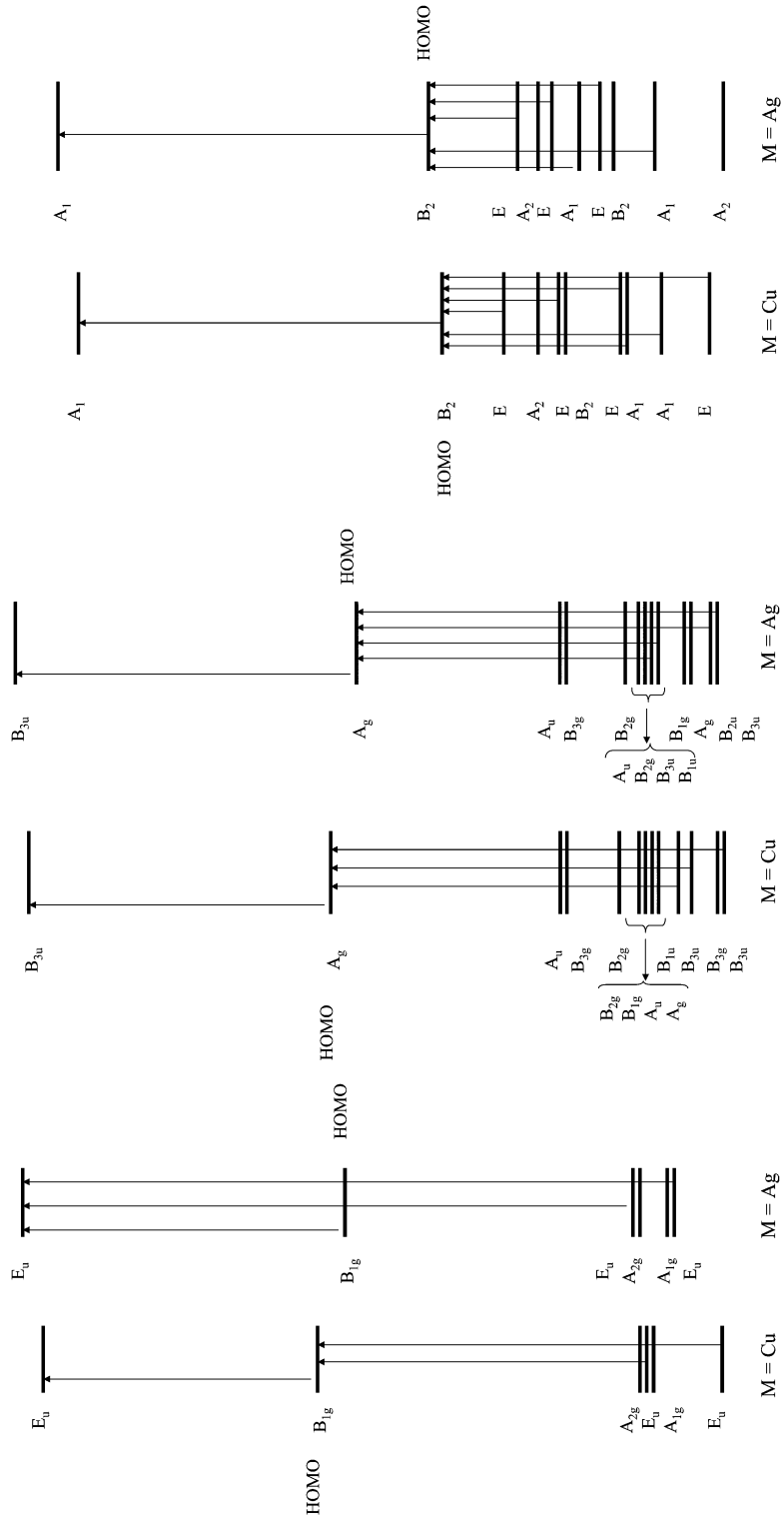


**Fig. 6** Summary of the optically allowed electronic transitions present in the three stable $[M(py)_4]^{2+}$ structures discussed in the text. The separation of levels is based on the energies at which orbitals appear in the calculations.

above the ground state ($D_{4h}$) are accessible, then favourable Franck-Condon factors could lower (red shift) some of the transitions out of the $D_{4h}$ structure by up to 2,000 $cm^{-1}$. However, even with this additional contribution, the only transitions that consistently fall within the above range are those out of the $D_{2d}$ structure. In addition to lying within the experimental band, several of the transitions also include a significant d-orbital contribution such that they could be considered, at least in part, as d–d transitions. This being the case then the subsequent decay process should be accompanied by the loss of a neutral ligand, which is precisely what is observed in the experiment. However, bearing in mind the results of Deeth[32] and Szilagyi *et al.*,[33] there is a strong possibility that our calculations have overestimated the degree of covalency present in the $[Cu(py)_4]^{2+}$ complex. In particular, the calculated percentage metal – ligand contributions given in Table 3 for each HOMO follows the pattern presented in Scheme 2A of ref. 33; in contrast, a more accurate description of the metal and ligand contributions to the HOMO would reduce d-orbital stability and, in turn, lower the energies of ligand field transitions. This being the case, then a number of possible d–d transitions could fall within the range covered by the experimental data.

In contrast to the case for copper(II), interpretation of the results for silver(II) is probably restricted on energy grounds to $D_{4h}$ and $D_{2h}$ geometries. As can be seen from Table 3, there are several transitions that fall within the range surveyed and these all lie at ~22,000 $cm^{-1}$, which is exactly where the experimental results reach a maximum. In addition, all of the transitions involve ligand-to-metal electron transfer, which in the experiment should lead to the loss of $py^+$, which again is precisely what is observed.

## Conclusion

New experimental data have been presented on ligand field photofragmentation spectra recorded in the gas phase for $[M(py)_n]^{2+}$ complexes, where M is either $Cu^{2+}$ or $Ag^{2+}$ and $n$ lies in the range 3–7. The results show a variety of photofragmentation patterns and wavelength dependences, many of which are successfully accounted for using density functional theory.

## Acknowledgements

The authors would like to thank EPSRC for financial support and for the award of research studentships to LP and GA. HC wishes to thank the EPSRC for the award of a university research fellowship. The Sussex High Performance Computing Initiative and the UK computational facilities at RAL are acknowledged for the provision of computer time.

## References

1 A. B. P. Lever, *Inorganic Electronic Spectroscopy*, Elsevier, Amsterdam, 2nd edn., 1984.
2 F. A. Cotton, G. Wilkinson, *Advanced Inorganic Chemistry*, Wiley, London, 1988.
3 M. A. Duncan, *Annu. Rev. Phys. Chem.*, 1997, **48**, 69.
4 J. J. R. Fraústo da Silva, R. J. P. Williams, *The Biological Chemistry of the Elements*, Clarendon Press, Oxford, 1997.
5 A. T. Blades, P. Jayaweera, M. G. Ikonomou and P. Kebarle, *Int. J. Mass Spectrom. Ion Processes*, 1990, **102**, 251; A. T. Blades, P. Jayaweera, M. G. Ikonomou and P. Kebarle, *J. Chem. Phys.*, 1990, **92**, 5900.
6 M. Peschke, A. T. Blades and P. Kebarle, *J. Phys. Chem. A*, 1998, **102**, 9978.
7 M. Peschke, A. T. Blades and P. Kebarle, *J. Am. Chem. Soc.*, 2000, **122**, 1492.
8 T. G. Spence, B. T. Trotter, T. D. Burns and L. A. Posey, *J. Phys. Chem. A*, 1998, **102**, 6101.
9 C. J. Thompson, J. Husband, F. Aguirre and R. B. Metz, *J. Phys. Chem. A*, 2000, **104**, 8155.
10 A. J. Stace, N. R. Walker and S. Firth, *J. Am. Chem. Soc.*, 1997, **119**, 10 239.
11 N. R. Walker, R. R. Wright and A. J. Stace, *J. Am. Chem. Soc.*, 1999, **121**, 4837.
12 N. R. Walker, R. R. Wright, P. E. Barran and A. J. Stace, *Organometallics*, 1999, **18**, 3569.
13 N. Walker, M. P. Dobson, R. R. Wright, P. E. Barran, J. N. Murrell and A. J. Stace, *J. Am. Chem. Soc.*, 2000, **122**, 11 138.
14 R. R. Wright, N. R. Walker, S. Firth and A. J. Stace, *J. Phys. Chem. A*, 2001, **105**, 54.
15 H. Cox, G. Akibo-Betts, R. R. Wright, N. R. Walker, S. Curtis, B. Duncombe and A. J. Stace, *J. Am. Chem. Soc.*, in print.
16 L. Puskar and A. J. Stace, unpublished results.
17 L. Puskar, P. E. Barran, R. R. Wright, D. A. Kirkwood and A. J. Stace, *J. Chem. Phys.*, 2000, **112**, 7751.

18 L. Puskar and A. J. Stace, *J. Chem. Phys.*, 2001, **114**, 6499.
19 D. L. Leussing and R. C. Hansen, *J. Am. Chem. Soc.*, 1957, **79**, 4270.
20 E. König and H. L. Schläfer, *Z. Phys. Chem. (Munich)*, 1960, **26**, 371.
21 H. L. Schläfer and E. König, *Z. Phys. Chem. (Munich)*, 1961, **30**, 145.
22 R. S. Banerjee and S. Basu, *J. Inorg. Nucl. Chem.*, 1964, **26**, 821.
23 H. G. Hecht and J. P. Frazier, *J. Inorg. Nucl. Chem.*, 1966, **29**, 613.
24 K. Ozutsumi and T. Kawashima, *Polyhedron*, 1992, **11**, 169.
25 M. Kurihara, T. Kawashima and K. Ozutsumi, *Z. Naturforsch.*, 2000, **55b**, 277.
26 *ADF 2.3.0*, Vrije Universiteit, Amsterdam.
27 G. Te Velde and E. J. Baerends, *J. Comput. Phys.*, 1992, **99**, 84.
28 S. H. Vosko, L. Wilk and N. Nusair, *Can. J. Phys.*, 1980, **58**, 1200.
29 A. D. Becke, *Phys Rev. A.*, 1988, **38**, 3098.
30 J. P. Perdew, *Phys Rev. B*, 1986, **33**, 8822.
31 O. Gunnarsson and B. I. Lundqvist, *Phys. Rev. B*, 1976, **13**, 4274.
32 R. J. Deeth, *J. Chem. Soc., Dalton Trans.*, 2001, 664.
33 R. K. Szilagyi, M. Metz and E. I. Solomon, *J. Phys. Chem. A*, 2002, **106**, 2994.
34 A. J. Jones, P. Jukes, A. Buxey and A. J. Stace, *J. Chem. Phys.*, 1997, **106**, 1367.
35 N. E. Levinger, D. Ray, K. K. Murray, A. S. Mullin, C. P. Schulz and W. C. Lineberger, *J. Chem. Phys.*, 1988, **89**, 71.
36 Z. Y. Chen, C. R. Albertoni, M. Hasegawa, R. Kuhn and A. W. Castleman Jr., *J.Chem. Phys.*, 1989, **91**, 4019.
37 N. L. Doltsinis and P. J. Knowles, *Chem. Phys. Lett.*, 1999, **301**, 241.
38 J. Bjerrum, C. J. Ballhausen and C. K. Jørgensen, *Acta Chem. Scand.*, 1954, **8**, 1275.
39 V. Romano and J. Bjerrum, *Acta Chem. Scand.*, 1970, **24**, 1551.
40 R. K. Murmann and F. Basolo, *J. Am. Chem. Soc.*, 1955, **77**, 3484.
41 W. E. Bull and L. E. Moore, *J. Inorg. Nucl. Chem*, 1965, **27**, 1341.
42 J. R. Wasson, *J. Inorg. Nucl. Chem.*, 1966, **28**, 2201.
43 T. Halpern, W. D. Phillips and J. A. McMillan, *J. Chem. Phys.*, 1970, **52**, 5548.
44 R. Åkesson, L. G. M. Pettersson, M. Sandström and U. Wahlgren, *J. Am. Chem. Soc.*, 1994, **116**, 8691.
45 D. W. Smith, *J. Chem. Ed.*, 1977, **54**, 540.
46 S. M. Nelson and T. M. Shepherd, *Inorg. Chem.*, 1965, **4**, 813.
47 G. J. Ferraudi, *Elements of Inorganic Photochemistry.*, John Wiley & Sons, New York, 1987.